Vacuum 136 (2017) 163–167

Contents lists available at ScienceDirect

Vacuum

journal homepage: www.elsevier.com/locate/vacuum

Comparison of measured and computed beam ion current densities emitted from two 2 kJ plasma focus machines

M. Akel [a, *], S. Alsheikh Salo [a], Sh. Ismael [a], S.H. Saw [b, c], S. Lee [b, d, e]

[a] Department of Physics, Atomic Energy Commission, PO Box 6091, Damascus, Syria
[b] Institute for Plasma Focus Studies, 32 Oakpark Drive, Chadstone, VIC 3148, Australia
[c] Nilai University, 1, Persiaran Universiti, Putra Nilai, 71800 Nilai, Malaysia
[d] Physics Department, University of Malaya, Kuala Lumpur, Malaysia
[e] INTI International University, 71800 Nilai, Malaysia

ARTICLE INFO

Article history:
Received 28 July 2016
Received in revised form
6 November 2016
Accepted 3 December 2016
Available online 5 December 2016

Keywords:
Ion beam properties
Plasma focus
Lee model
Nitrogen gas

ABSTRACT

Computed results of beam ion current density are compared with the measured values for a range of pressures (0.13–1.33 mbar) and a range of distances (3–9 cm) downstream of the plasma compression commonly called the pinch in literature dealing with electromagnetically compressed dense plasmas. Partial agreement is found to an extent not reported before. Computed and measured values of ion current densities of the order of 10^7 Am^{-2} are found. Moreover the results indicate that detectors should not be placed closer than two anode radii from the position of the plasma focus pinch to avoid interference with the pinch dynamics. The maximum power flow density is found to range from 10^{12} to 10^{14} Wm^{-2}. The damage factor (heat flux factor) reach 10^9 - 10^{10} $Wm^{-2}s^{0.5}$ at the pinch exit, while the power flow densities and damage factor values decrease to around 10^{10} Wm^{-2} and 10^6 $Wm^{-2}s^{0.5}$, respectively, at the distances from the anode top more than 6 cm.

1. Introduction

Plasma focus devices are used as a source of multi-radiation including neutrons, soft and hard x-rays [1–3], relativistic energy electrons [4] and fast ion beams [5,6] in applications such as electron and soft x-ray lithography [7], x-rays backlighting [8], biological radiography [3], fabricating composite and specialized films [9–11]. Plasma focus operated with nitrogen is an ion source for material applications [12–18]. The ion flux from plasma focus (PF) with various working nitrogen pressures is measured using Faraday Cup (FC). It is found that the ion flux ranges from 4.34×10^{16}–1.86×10^{17} ions/sterad for energy range of 3–12 keV, skewed towards the low energy ions. The efficiency can be optimized by adjusting the operational gas pressures [19]. The ion beam energy may be measured using time of flight method [20]. A Mather type 2.3 kJ PF was used with 1.25 mbar of nitrogen for the treatment of titanium samples at distances from the pinch (from 3 to 9 cm). The energetic ions were characterized with a BPX65 diode. The results showed that the ion current density decreased from 1.4×10^7 Am^{-2} to 1.1×10^7 Am^{-2} as the diode was moved from 3 to 9 cm [5]. In another experiment [6], 3 F cups were used at various angular positions at 6 cm from the anode tip. The results show that the average ion current density estimated for the solid anode changed with the gas pressure from 1.15×10^7 Am^{-2} (at 0.13 mbar of nitrogen) to 0.6×10^7 Am^{-2} (at 1.33 mbar of nitrogen) with the maximum value of 1.25×10^7 Am^{-2} (at 0.7 mbar of nitrogen) [6]. Ion beams of nitrogen were studied [21] with different pressures in a 2.3 kJ energy using CR-39 SSNTDs, finding 10^6 tracks/cm^2. H. Kelly et al. [22] used Faraday Cup and Thomson spectra in PF II (4.75 kJ, 30 kV) and recorded 3.2×10^{13} ions/sterad with energy content of 0.74 J/sterad, measuring ion energies in range 50–1000 keV. Sohrabi et al. [23] studied the angular distribution of nitrogen ion tracks using mains frequency electrochemical etching of large-area polycarbonate (PC) detectors. The results from their 4 kJ PF showed an energy-dependent asymmetrical ion angular using the PC method and also a Faraday Cup (FC) method. The maximum ion density were estimated to be 10^{11} ions m^{-2} and 10^{25} ions m^{-2}, respectively from the polycarbonate (PC) and the Faraday Cup (FC) methods [24]. It needs to be noted that the method employed using Polycarbonate (PC) track detectors only measures a fraction of the total number of beam ions so that the very small ion number densities measured by polycarbonate (PC) track detectors are not

* Corresponding author.
E-mail address: pscientific14@aec.org.sy (M. Akel).

http://dx.doi.org/10.1016/j.vacuum.2016.12.005
0042-207X/

unexpected. Nitrogen ion implantation into titanium was studied [25] using 300–400 ns ion pulses. Compositional and physical changes in the near surface region were found ascribed to heating with accumulated ion fluences of 10^{18} - 10^{20} m^{-2}. Sanchez et al. [26] investigated the temperature profile and evolution of the sample surfaces upon the ion implantation into titanium, stainless steel and copper with ion beams from a plasma focus device. Four different anode tips were used to study ion distributions. The maximum ion flux of 6×10^{12} ions/steradian is obtained with cylindrical anode tip that increases to 10^{13} ions/steradian for conical anode tip [27]. It seems that the ion beam measurements on plasma focus have produced a variety of results using different units. To produce a clearer picture, the Lee model has been modified based on a mechanism proposed by Gribkov et al. [28–30]. This code has been used to study ion beams from plasma focus [31–37].

In this paper, we carry out ion calculations on two small plasma focus devices. The calculations are compared with measurements which have been reported from these devices.

2. Theory and procedure

The properties of the ion beam are computed following Lee and Saw [31, 32] using the Lee code extended for ion calculations, the RADPF.FIB. In the code, we propose that in the plasma focus the narrow ion beam exits the pinch along its axis (having the same cross-section as the pinch) with little divergence; at least until it overtakes the post-pinch axial shock wave. The exit beam is best characterized by the ion number per unit cross-section which we term the fluence. we use the following equations [32]:

$$\text{Flux}\left(\text{ions m}^{-2}\text{s}^{-1}\right) = J_b = 2.75 \times 10^{15}\left(f_e \Big/ \left[M Z_{eff}\right]^{1/2}\right)\left\{ \times \left(\ln[b/r_p]\right) \Big/ \left(r_p{}^2\right)\right\}\left(I_{pinch}{}^2\right) \Big/ U^{1/2} \quad (1)$$

$$\text{Fluence}\left(\text{ions m}^{-2}\right) = 2.75 \times 10^{15}\tau\left(f_e \Big/ \left[M Z_{eff}\right]^{1/2}\right)\left\{ \times \left(\ln[b/r_p]\right) \Big/ \left(r_p{}^2\right)\right\}\left(I_{pinch}{}^2\right) \Big/ U^{1/2} \quad (2)$$

where M = 14 for nitrogen, $f_e = 0.14$ (the fraction of energy converted from pinch inductive energy PIE into beam kinetic energy BKE) is equivalent to ion beam energy of 3%–6% E_0 (E_0 - the storage energy) for cases when the PIE holds 20%–40% of E_0 as observed for low inductance PF. The diode voltage U is $U = 3V_{max}$ taken from data fitting in extensive earlier numerical experiments, where V_{max} is the maximum induced voltage of the pre-pinch radial phase. The value of the ion flux is deduced in each situation for specific machine using specific gas by computing the values of effective charge Z_{eff}, pinch radius r_p, pinch duration τ, pinch current I_{pinch} and U by configuring the Lee Model code with the parameters of the specific machine and specific gas.

Once the flux is determined, the following quantities are also computed:

- Energy flux or power density flow (Wm^{-2}) is computed from $\mathbf{J_b} \times Z_{eff}U$ noting the need to multiply by 1.602×10^{-19} to convert eV to J;
- Power flow (W) is computed from Energy flux × pinch cross-section;
- Current density (Am^{-2}) is computed from $\mathbf{J_b}$ × ion charge eZ_{eff};
- Current (A) is computed from Current density × pinch cross-section;
- Ions per sec (ions s^{-1}) is computed from $\mathbf{J_b}$ × pinch cross-section;
- Fluence (ions m^{-2}) is computed from $\mathbf{J_b} \times \tau$;
- Energy fluence (J m^{-2}) is computed from $\mathbf{J_b} \times \tau \times Z_{eff}U$;
- Number of ions in beam (ions) is computed from Fluence × pinch cross-section;
- Energy in beam (J) is computed from Number of ions in beam × $Z_{eff}U$;
- Damage Factor ($Wm^{-2}s^{0.5}$) is computed from $\mathbf{J_b} \times Z_{eff}U \times \tau^{0.5}$ and Energy of fast plasma stream (J).

Experimentally it is found that as the focus pinch starts to break up a fast shock wave exits the plasma focus pinch in the axial direction preceding the ion beams which rapidly catches up and overtakes it. Associated with this fast post-pinch axial shock wave is a fast plasma stream (FPS). We estimate the energy of the FPS by computing the work done by the magnetic piston through the whole radial phase from which is subtracted twice the ion beam energy (the second count being for the oppositely directed relativistic electron beam) and from which is further subtracted the radiation yield of the plasma pinch. We also need to emphasize that the calculations of this work pertain to the ion beam at the exit of the pinch. At a distance from the pinch, the propagating ion beam will be attenuated by interaction with the medium traversed and also by beam and stream divergence. The practical importance of these attenuation effects demands further study.

The code is configured to work as any plasma focus device (Fig. 1a and b) by inputting the bank parameters: static inductance (L_0), storage capacitance (C_0) and stray circuit resistance (r_0); the

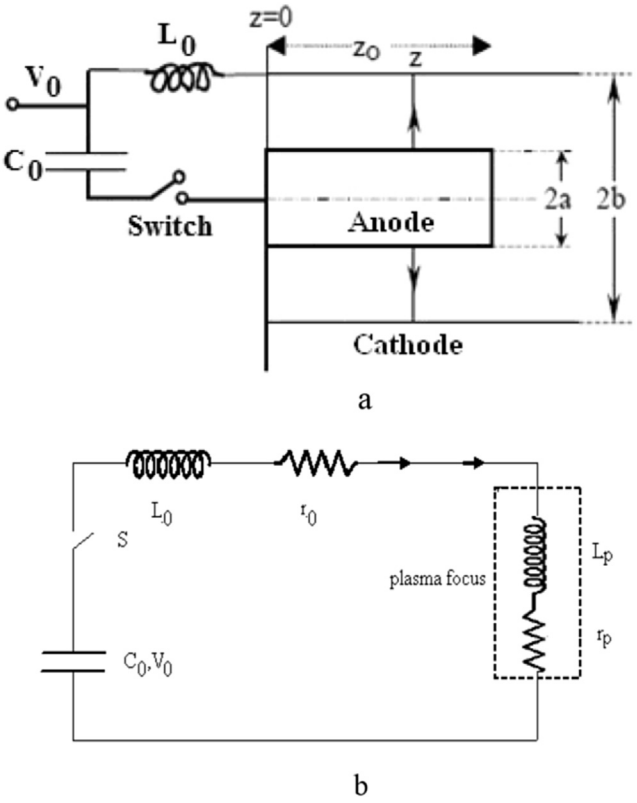

Fig. 1. a - The main parts of plasma focus device are as shown on the schematic diagram; b - Equivalent electrical circuit of the plasma focus device; where L_p and r_p are time-varying inductance and resistance of the plasma focus.

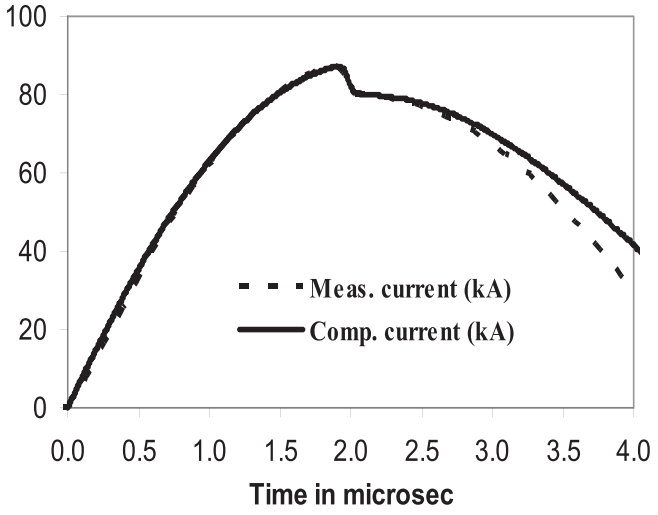

Fig. 2. Computed discharge current compared to published current for 2.2 kJ PF operated with 0.4 mbar nitrogen.

tube parameters: cathode radius (b), anode radius (a), tube axial length (z_0) and operational parameters: operating voltage (V_0), operating initial pressure (p_0). The computed total current waveform is fitted to an experimentally measured current, by Rogowski coil, using four model parameters representing the mass swept-up factor f_m, the plasma current factor f_c for the axial phase and the mass swept-up factor f_{mr} and the plasma current factor f_{cr} for the radial phases. From experience it is known that the current trace of the focus is one of the best indicators of gross performance. The axial and radial phase dynamics and the crucial energy transfer into the focus pinch are among the important information that is quickly apparent from the current trace. The exact time profile of the total current trace is governed by the bank parameters, by the focus tube geometry and the operational parameters. It also depends on the fraction of mass swept-up and the fraction of sheath current and the variation of these fractions through the axial and radial phases. These parameters determine the axial and radial dynamics, specifically the axial and radial speeds which in turn affect the profile and magnitudes of the discharge current. The detailed profile of the discharge current during the pinch phase also reflects the Joule heating and radiative yields. At the end of the pinch phase the total current profile also reflects the sudden transition of the current flow from a constricted pinch to a large column flow. Thus the discharge current powers all dynamic, electrodynamics, thermodynamic and radiation processes in the various phases of the plasma focus. Conversely all the dynamic, electrodynamics, thermodynamic and radiation processes in the various phases of the plasma focus affect the discharge current. It is then no exaggeration to say that the discharge current waveform contains information on all the dynamic, electrodynamics, thermodynamic and radiation processes that occurs in the various phases of the plasma focus. This explains the importance attached to matching the computed current trace to the measured current trace in the procedure adopted by the Lee Model code. Once fitted the code outputs realistic the following data: dynamics and energy content of the phases, pinch geometry, temperatures and densities, line radiation and neutron yields, ion beam properties, fast plasma stream dynamics and energies [37–39].

More detailed information about the Lee code is given in ref. 39 and more detailed information about the ion beam calculations is given in [31, 32].

3. Numerical calculations: results and discussion

The Lee model is configured to operate as the 2.2 kJ PF plasma focus device [6, 40] for nitrogen ion beam calculations, and the reasonably good fit is obtained with the following bank and tube parameters (L_0, C_0 and z_0 fitted and r_0 fitted) are used:

Bank parameters: $L_0 = 330$ nH, $C_0 = 7.1$ μF, $r_0 = 62$ mΩ.
Tube parameters: b = 4 cm, a = 1.05 cm, $z_0 = 12.5$ cm.
Operating parameters: $V_0 = 25$ kV, $P_0 = 0.4$ mbar Nitrogen.
together with the following fitted model parameters:

$$f_m = 0.014,\ f_c = 0.7,\ f_{mr} = 0.15 \text{ and } f_{cr} = 0.7$$

The fitted computed current waveform is compared with published waveform in Fig. 2.

Then for studying of the pressure effects on the ion beam properties, these fitted values of the model parameters are used at range of pressures (see Table 1).

Table 1 reveals that ion flux increases with pressure with maximum 3.1×10^{27} ions $m^{-2}s^{-1}$ at 1.33 mbar. The maximum value of the fluence is 45×10^{18} ions m^{-2} at 1.33 mbar. The beam ion number varies from 3.8×10^{13} to 15×10^{13} for 2.2 kJ PF. Our results show that power flow density has a peak value of 11.3×10^{13} Wm^{-2} at 0.4 mbar, and the maximum value of the damage factor is 11.6×10^{9} $Wm^{-2}s^{0.5}$ at 0.7 mbar. The values mentioned above are at pinch exit. The ion beam typically interacts with the medium traversed and is also diminished in intensity by beam divergence. Energy loss due to interactions with background gas is negligible [41].

We consider a divergence of 40° [24, 26, 27] and use the formula [42] $f_i = \frac{N_i}{\sigma_R}$ Here N_i is the computed ion number and $\sigma_R = \pi(R \tan \theta)^2$ - beam cross-sections, assumed circular, at distance R from the exit point, θ - half angle. Their measurements give the average ion current density from 1.15×10^7 Am^{-2} (at 0.13 mbar of nitrogen) to 0.6×10^7 Am^{-2} (at 1.33 mbar of nitrogen) with the maximum value of 1.25×10^7 Am^{-2} (at 0.7 mbar of nitrogen) [6]. Numerical experiments are carried out on 2.2 kJ PF [6] and 2.3 kJ PF [5] versus pressure and compared with the measured average ion current density for the solid anode results at 6 cm from the anode top (see Fig. 3).

From Fig. 3, it is noticed that there is fair agreement between

Table 1
Nitrogen ion beam properties versus pressure in 2.2 kJ PF at the pinch exit (R = 0 cm).

p_0 (mbar)	Ion fluence ($\times 10^{18}$ m^{-2})	Ion flux ($\times 10^{27}$ m^{-2} s^{-1})	Ion energy (keV)	Ion number ($\times 10^{13}$)	Current density ($\times 10^{9}$ Am^{-2})	Power flow density ($\times 10^{13}$ Wm^{-2})	Damage factor ($\times 10^{9}$ $Wm^{-2}s^{0.5}$)
0.13	8.5	1.2	381	3.8	1.30	7.1	6.1
0.27	16	1.9	340	6.0	2.11	10	9.6
0.4	22	2.3	312	7.5	2.53	11.3	11.1
0.7	30	2.7	256	9.9	2.85	11	11.6
0.94	3.7	2.9	211	12	2.93	10	11.2
1.33	45	3.1	164	14	2.82	8	9.7
1.6	43	2.6	139	15	2.35	6	7.5

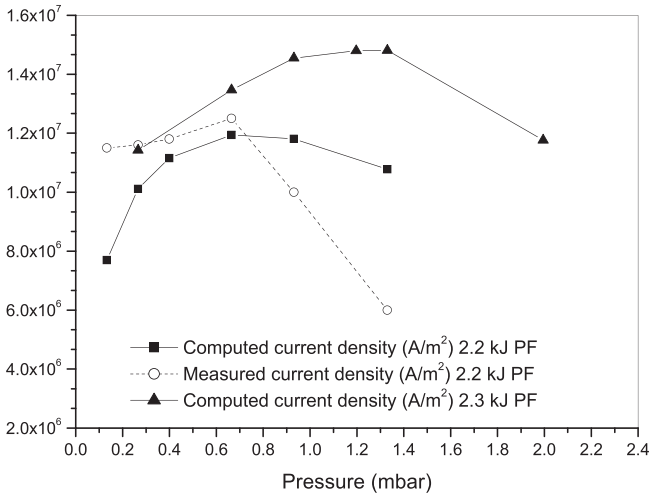

Fig. 3. Comparison of the computed (2.2 kJ PF and 2.3 kJ PF) ion current density with the measured in the 2.2 kJ PF at 6 cm distance of the anode top versus nitrogen pressure.

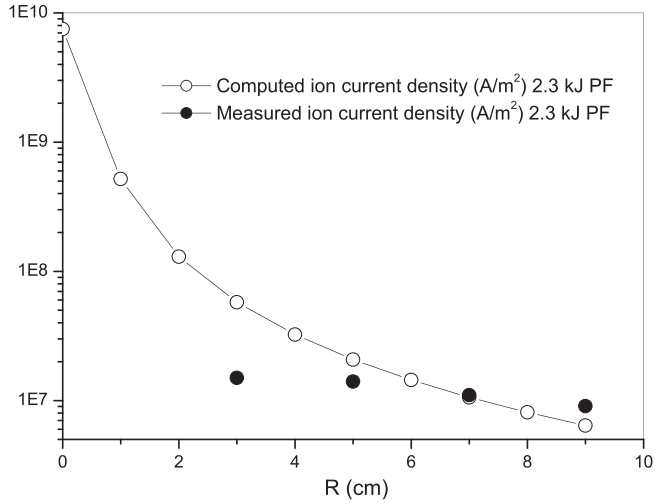

Fig. 4. Comparison of the computed and measured ion current density in the 2.3 kJ PF at 1.25 mbar nitrogen placed at different distances from the anode tip.

the calculated and measured ion current density for low pressures up to 0.8 mbar. Beyond 0.8 mbar up to 1.33 mbar and above, the measured values fall more than the computed. At 1.33 mbar, the computed value is about half of the measured for the 2.2 kJ PF. Agreement, even partial, to this level over a range of pressures has not been reported before. Table 2 presents the ion beam properties emitted from 2.2 kJ PF versus gas pressure at 6 cm from the anode top.

Table 2 shows that the ion flux reaches a maximum (11.85×10^{24} ions $m^{-2}s^{-1}$) at 0.94 mbar and the current density has a maximum (1.2×10^{7} Am^{-2}) at 0.7 mbar. Our results show that maximum power flow density reaches 7×10^{10} Wm^{-2} at 0.4 mbar and the implantation mode of irradiation [28] is dominant in the 2.2 kJ PF for the target placed at 6 cm from the anode tip. Damage factor reaches 7.2×10^{6} $Wm^{-2}s^{0.5}$ at a pressure of 0.7 mbar. These results show the effects of distance from the anode top on the ion beam properties and on the material processing regimes.

Ion beam properties at different locations from the anode tip are also investigated for a second PF operated with 1.25 mbar nitrogen 2.3 kJ PF [5], for nitriding titanium samples placed at locations varying from 3 to 9 cm. The experimental results showed that the ion current density decreases from 1.4×10^{7} Am^{-2} at 3 cm to 1.1×10^{7} Am^{-2} at 9 cm on the axial position. Our Numerical results on 2.3 kJ PF are compared with the measured results at 1.25 mbar for different distances from the anode top (see Fig. 4).

Table 3 presents the properties of ions emitted from 2.3 kJ PF operated at 1.25 mbar nitrogen for different distances from the tip of the anode.

Table 3 shows that the ion flux decreases from 6.7×10^{27} ions $m^{-2}s^{-1}$ at the pinch to 5.71×10^{24} ions $m^{-2}s^{-1}$ at 9 cm. The current density ranges from a maximum 7.5×10^{9} Am^{-2} at the pinch exit to 6.4×10^{6} Am^{-2} at a 9 cm distance. The calculations show that power flow density in the pinch exit reaches 4.7×10^{14} Wm^{-2} at 1.25 mbar, and reduces with the distance to 5.53×10^{10} Wm^{-2}. Some partial agreement of the computed beam ion current density with the measured is observed between 5 cm and 9 cm. At a distance of 3 cm the measured value is significantly below the computed value. This could be due to the interference of the diode detector head with the plasma focus pinching dynamics when the detector head is placed at a distance within two 'anode radii' from the pinch. These results could reasonably indicate that detectors should not be placed at a distance less than two 'anode radii' from the expected position of the focus pinch.

4. Conclusion

Ion beam properties of nitrogen plasma focus at the pinch exit and at the various axial position from the anode top are studied and discussed. The maximum fluence vary over the range 10^{18} - 10^{19} ions m^{-2} at the pinch exit and reduce to 10^{16} to 10^{17} ions m^{-2} at distances more than 6 cm from the end of the anode. Computations show the power flow density range from 10^{12} - 10^{14} Wm^{-2} and the damage factor range over 10^{9} - 10^{10} $Wm^{-2}s^{0.5}$ at the pinch exit, while the power flow densities and damage factor decreases to 10^{10} Wm^{-2} and 10^{6} $Wm^{-2}s^{0.5}$, respectively, at the distances from the anode top of more than 6 cm. Our computed results of beam ion current density are compared with the measured values for a range of pressures (0.13–1.33 mbar) and a range of distances (3–9 cm) downstream of the pinch. Some partial agreement is found to an extent not reported before. Computed and measured values of

Table 2
Nitrogen ion beam properties emitted from 2.2 kJ PF at 6 cm from the anode top.

p_0 (mbar)	Ion fluence ($\times 10^{16}$ m^{-2})	Ion flux ($\times 10^{24}$ m^{-2} s^{-1})	Current density ($\times 10^{7}$ Am^{-2})	Power flow density ($\times 10^{10}$ Wm^{-2})	Damage factor ($\times 10^{6}$ $Wm^{-2}s^{0.5}$)
0.13	5.0	6.86	0.76	5.96	5.09
0.3	7.8	9.01	1.01	6.97	6.50
0.4	9.6	9.94	1.12	7.04	6.93
0.7	12	11.22	1.19	6.82	7.19
0.94	14.9	11.85	1.18	6.28	7.05
1.33	17.1	11.66	1.08	5.11	6.18
1.6	17.8	11	0.98	3.99	5.08

Table 3
Variation of nitrogen ion beam properties in 2.3 kJ PF at 1.25 mbar nitrogen for different locations from the tip of the anode.

R (cm)	Ion fluence ($\times 10^{17}$ m^{-2})	Ion flux ($\times 10^{25}$ m^{-2} s^{-1})	Current density ($\times 10^{7}$ Am^{-2})	Power flow density ($\times 10^{11}$ Wm^{-2})	Damage factor ($\times 10^{7}$ Wm^{-2} $s^{0.5}$)
0	527	672	753	4666	4132
1	36.1	46.2	51.98	45.7	40.4
2	9.02	11.5	12.9	11.4	10.1
3	4.01	5.14	5.76	5.05	4.46
4	2.25	2.89	3.24	2.83	2.50
5	1.44	1.85	2.07	1.81	1.59
6	1.00	1.28	1.44	1.25	1.17
7	0.73	0.95	1.05	0.92	0.82
8	0.56	0.73	0.81	0.7	0.62
9	0.45	0.57	0.64	0.55	0.49

beam ion current densities of the order of 10^7 Am^{-2} are found over the range of conditions in two separate series of experiments in two plasma focus machines. Moreover comparison of computed beam ion current density with that measured from a 2.3 kJ plasma focus shows reasonable agreement when the detector head is placed beyond two 'anode radii' from the end of the plasma focus pinch with both measured and computed values in the region of 10^7 Am^{-2} between 5 and 9 cm downstream from the end of the anode. When the detector was located at 3 cm from anode top the measured value of the beam ion current density was much less than the measured. This indicates that detectors should not be placed too close to the pinch in order not to interfere with the pinch dynamics. The consistency of measured and computed results adds limited confidence to the computations of the Lee code applied to beam ion properties [31–33] although clearly further improvement needs to be made.

Acknowledgment

The authors acknowledge Director General of AECS, for permanent support and encouragement. SL and SHS records support of IAEA CRP F1.30.13 (RC 16934) and FRGS-2-2013/SG02-INTI/01/1.

References

[1] R. Verma, et al., IEEE trans. Plasma Sci. 40 (2012) 3280.
[2] N.K. Neog, S.R. Mohanty, Journal of applied physics 99 (2006) 013302.
[3] F. Castillo-Mejia, et al., IEEE trans. Plasma Sci. 29 (2001) 921.
[4] A. Patran, et al., Plasma Sources Sci.Technol 14 (2005) 549.
[5] M. Hassan, et al., J. Phys. D. Appl. Phys. 40 (2007) 769.
[6] S.R. Mohanty, et al., Jpn. J. Appl. Phys. 46 (2007) 3039.
[7] P. Lee, et al., Plasma Sources Sci. Technol. 6 (1997) 343.
[8] M. Zakaullah, et al., IEEE Trans. Plasma Sci. 30 (2002) 2089.
[9] I.A. Khan, et al., Nucl. Instru. Meth. Phys. Res. B 268 (2010) 2228.
[10] T. Hussain, et al., Nucl. Instru. Meth. Phys. Res. B 267 (2009) 768.
[11] S. Jabbar, et al., J. Vac. Sci. Technol. A 27 (2) (2009) 381.
[12] M. Ahmad, S. Al-Hawat, M. Akel, J. Fusion Energy 32 (4) (2013) 471–478.
[13] M. Ahmad, Sh Al-Hawat, M. Akel, O. Mrad, J. Appl. Phys. 117 (2015) 063301.
[14] R.S. Rawat, J. Phys. Conf. Ser. 591 (2015) 012021.
[15] Kin Seng Tan, Rui Jing Mah, Rajdeep Singh Rawat, IEEE Trans. Plasma Sci. 43 (2015) 2539.
[16] Mohammad Taghi Hosseinnejad, Zohreh Ghorannevis, Mahmood Ghoranneviss, G. Reza Etaati, Marzieh Shirazi, J. Fusion Energy 34 (6) (2015) 1217–1228.
[17] Jamil Siddiqui, Tousif Hussain, Riaz Ahmad, Waris Ali, Ali Hussnain, Rana Ayub, J. Fusion Energy 34 (5) (2015) 1193–1202.
[18] Jamil Siddiqui, Tousif Hussaina, Riaz Ahmad, Nida Khalid, Chin. Phys. B 24 (2015) 065204. No. 6.
[19] H.A. R Tariq, et al., PK ISSN 0022-2941, CODEN JNSMAC 48 (2008) 65, 1 & 2.
[20] (M.Sc. Thesis) M.A. I Elgarhy, et al., Plasma Focus and its Applications, Cairo, 2010.
[21] R. Ahmad, et al., J. Fusion Energy 21 (2002) 217.
[22] H. Kelly, et al., IEEE Trans. Plasma Sci. 26 (1998) 113.
[23] M. Sohrabi, M. Habibi, G.H. Roshani, V. Ramezani, Radiat. Meas. 47 (2012) 530–536.
[24] M. Sohrabi, M. Habibi, H.R. Yousefi, G.H. Roshani, Contrib. Plasma Phys. 53 (3) (2013).
[25] J.N. Feugeas, et al., Rad. Eff. Defects Solids 25 (1993) 1.
[26] G. Sanchez, et al., Surf. Coat. Technol. 70 (1995) 181.
[27] Morteza Habibi, 380, Phys. Lett. A 380 (3) (2016) 439–443.
[28] V. A.Gribkov, A. Banaszak, B. Bienkowska, A.V. Dubrovsky, I. Ivanova-Stanik, L. Jakubowski, L. Karpinski, R.A. Miklaszewski, M. Paduch, M.J. Sadowski, M. Scholz, A. Szydlowski, K. Tomaszewski, J. Phys. D. Appl. Phys. 40 (2007) 3592.
[29] V.N. Pimenov, Elena V. Demina, Sergey A. Maslyaev, Lev I. Ivanov, Vladimir A. Gribkov, Alexander V. Dubrovsky, Ülo Ugaste, Tõnu Laas, Marek Scholz, Ryszard Miklaszewski, Blagoslav Kolman, Agostino Tartari, Nukleonika 53 (3) (2008) 111–121.
[30] V.A. Gribkov, Plasma Phys. Control. Fusion 57 (2015) 065010.
[31] S. Lee, S. H Saw, Phys. Plasmas 19 (2012) 112703.
[32] S. Lee, S. H Saw, Phys. Plasmas 20 (2013) 062702.
[33] M. Akel, S. Alsheikh Salo, S.H. Saw, S. Lee, J. Fusion Energy 33 (2) (2014) 189–197.
[34] M. Akel, S. Alsheikh Salo, S.H. Saw, S. Lee, Vacuum 110 (2014) 54–57.
[35] M. Akel, S. Alsheikh Salo, S.H. Saw, S. Lee, IEEE Trans. Plasma Sci. 42 (9) (2014) 2202–2206.
[36] M. Akel, S. Alsheikh Salo, Sh Ismael, S.H. Saw, S. Lee, Physics of plasmas 21 (2014) 072507.
[37] S Lee, http://www.plasmafocus.net (2016).
[38] S. Lee, S. H Saw, J. Fusion Energy 27 (2008) 292–295.
[39] S. Lee, J. Fusion Energy 33 (4) (2014) 319–335.
[40] S.R. Mohanty, et al., Jpn. J. Appl. Phys. 44 (7A) (2005) 5199.
[41] http://www.srim.org (SRIM-2013 – (Range of Ions).
[42] G. Sanchez, J. Feugeas, J. Pys. D. Appl. Phys. 30 (1997) 927.